ACS SENSORS

pubs.acs.org/acssensors Article

Aptamer–Antibody Chimera Sensors for Sensitive, Rapid, and Reversible Molecular Detection in Complex Samples

Dehui Kong,[#] Ian A. P. Thompson,[#] Nicolo Maganzini,[#] Michael Eisenstein, and Hyongsok Tom Soh*

Cite This: https://doi.org/10.1021/acssensors.3c01638 Read Online

ACCESS | Metrics & More | Article Recommendations | Supporting Information

ABSTRACT: The development of receptors suitable for the continuous detection of analytes in complex, interferent-rich samples remains challenging. Antibodies are highly sensitive but difficult to engineer in order to introduce signaling functionality, while aptamer switches are easy to construct but often yield only a modest target sensitivity. We present here a programmable antibody and DNA aptamer switch (PANDAS), which combines the desirable properties of both receptors by using a nucleic acid tether to link an analyte-specific antibody to an internal strand-displacement (ISD)-based aptamer switch that recognizes the same target through different epitopes. The antibody increases PANDAS analyte binding due to its high affinity, and the effective concentration between the two receptors further enhances two-epitope binding and fluorescent aptamer signaling. We developed a PANDAS sensor for the clotting protein thrombin and show that a tuned design achieves a greater than 300-fold enhanced sensitivity compared to that of using an aptamer alone. This design also exhibits reversible binding, enabling repeated measurements with a temporal resolution of ∼10 min, and retains excellent sensitivity even in interferent-rich samples. With future development, this PANDAS approach could enable the adaptation of existing protein-binding aptamers with modest affinity to sensors that deliver excellent sensitivity and minute-scale resolution in minimally prepared biological specimens.

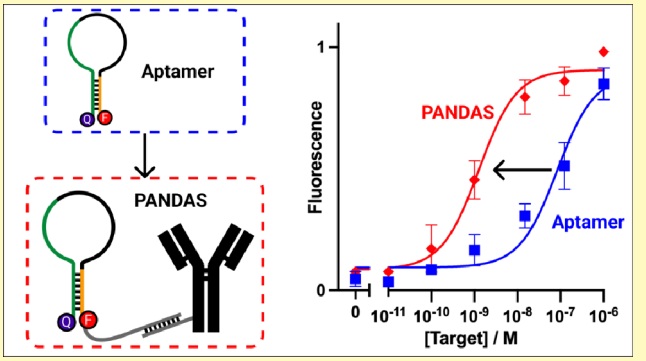

KEYWORDS: *continuous biosensing, structure-switching aptamer, antibody, fluorescent sensing, molecular recognition*

Most approaches to molecular detection are designed for single-time point measurements, but there is considerable value in being able to track changes in analyte concentration dynamically. This is particularly important when tracking clinically relevant markers in biofluids, where continuous measurements can provide a real-time indicator of disease states,[1,2] metabolic activity,[3] hormonal dysfunction,[4,5] and other physiological processes.[6,7] However, it remains a challenge to develop simple and generalizable biosensor architectures that are suitable for continuous molecular detection. Monoclonal antibodies generally offer the best sensitivity and specificity, but conventional immunoassays such as enzyme-linked immunosorbent assays (ELISA) require the use of a secondary reporter antibody and thus are limited to single-time point measurements.[8,9] One recently described alternative approach converts antibodies into a molecular pendulum construct that achieves reversible binding-induced electrochemical signaling.[10] However, this approach relies on the antibody's intrinsic properties and thus has limited capacity for tunability to optimize its sensitivity. In contrast to antibodies, it is relatively straightforward to engineer and tune nucleic-acid-based aptamers to undergo a reversible conformation change and signaling upon target binding. When coupled with redox tags as reporters, electrochemical aptamer-based molecular switches have been used to continuously measure target molecule concentrations directly in complex samples.[11−15] Molecular detection has also been achieved using fluorescence-based aptamer switches, also termed aptamer beacons, and this approach has achieved both single-time point and continuous molecular quantification for a range of target biomarkers, including detection in complex biofluids.[16−20] More general fluorescent aptamer switch architectures offer approaches to ensure structure switching and tune the affinity of the resulting switch, such as the intramolecular strand displacement (ISD) design, which introduces a complementary DNA strand to compete with the aptamer binding pocket.[21,22] Nevertheless, aptamer switch design approaches introduce important trade-offs, as competition- or unfolding-based switching mechanisms can greatly reduce aptamer affinity.[23] Given that aptamers generally

Received: August 8, 2023
Revised: January 18, 2024
Accepted: February 6, 2024

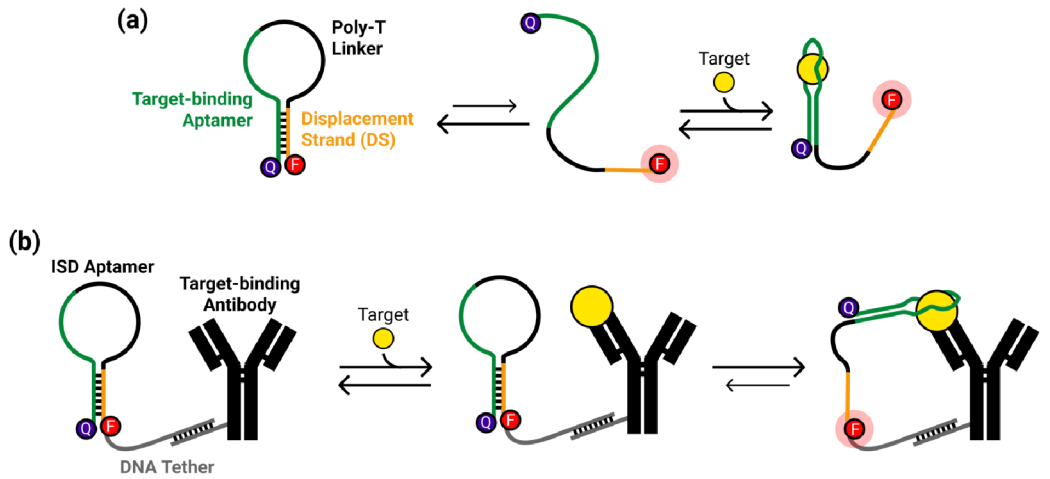

Figure 1. (a) Schematic of the intramolecular strand displacement (ISD) aptamer switch mechanism. In the ISD switch, an aptamer is linked to a partially complementary displacement strand (DS) via a poly-T linker, and the two ends of the DNA molecule are labeled with a fluorophore and a quencher moiety. Target binding leads to release of the DS and physical separation of these two elements, resulting in increased fluorescence. (b) Schematic of the programmable antibody and DNA aptamer switch (PANDAS) mechanism. In the PANDAS design, the ISD aptamer is coupled to the Fc domain of an antibody by a 30 nt oligonucleotide tether. The antibody will generally have a much higher affinity than the aptamer, increasing the probability of PANDAS binding to the free target at low concentrations, and thus the probability of the ISD aptamer binding and undergoing a conformational change that produces a fluorescent readout.

exhibit a lower target affinity than antibodies, this can render them insufficiently sensitive for real-world detection applications. While there are alternative strategies for designing structure-switching aptamers such as screening or truncation, these strategies all tend to yield aptamers with limited sensitivity that is generally inadequate for clinically relevant protein biomarkers, which often exhibit physiological concentrations in the subnanomolar range.[24]

In this work, we present a molecular switch design that leverages both the high affinity of antibodies and the molecular switch functionality that is accessible with aptamers. Our programmable antibody and DNA aptamer switch (PANDAS) design links a structure-switching aptamer to the Fc-region of a modified antibody through a short DNA scaffold such that the two affinity reagents bind separate epitopes of the target. Signaling is achieved through an ISD aptamer[21,22] design with a fluorescent readout. Normally, such sensors exhibit modest target affinity, but in the context of PANDAS, the affinity of the ISD aptamer is greatly enhanced through the effects of two-epitope binding. The antibody's high affinity relative to the aptamer and the high effective concentration between the aptamer and antibody means that the PANDAS construct binds targets at lower concentrations than the aptamer alone, and that there is a high degree of aptamer fluorescent signaling upon target binding to either receptor within PANDAS. As a demonstration, we have generated a PANDAS-based sensor for the blood clotting protein thrombin. We show that a highly tuned version of this construct can achieve >300-fold enhanced thrombin affinity and limit of detection relative to the aptamer switch on its own. Importantly, the ISD design also confers the ability to tune sensor affinity by altering the length of the displacement strand, and we show that an optimally tuned version of this PANDAS can achieve an effective equilibrium dissociation constant (K_D) of ~100 pM with a minimal background. Furthermore, this PANDAS construct binds reversibly, enabling us to obtain continuous measurements of changing thrombin concentrations with ~10 min temporal resolution. Finally, our sensor design maintains excellent target specificity and exhibits robust sensitivity and temporal resolution even when tested in an interferent protein-rich sample matrix. Given the modular design of the PANDAS construct, which requires no meaningful engineering of either the antibody or aptamer sequence beyond the introduction of a linker domain and displacement strand sequence, we believe that this strategy should be broadly applicable for repurposing low-affinity aptamer switches to detect low-abundance targets in complex samples.

RESULTS AND DISCUSSION

Rationale and Design for an Antibody-Enhanced Aptamer Switch. The PANDAS reagent design takes advantage of the benefits of both aptamer switches and monoclonal antibodies. The aptamer component of the PANDAS construct makes use of the ISD design to achieve fluorescent signaling upon aptamer-target binding (Figure 1a). Here, the aptamer is linked to a short displacement strand (DS) domain that is complementary to a portion of the aptamer's binding motif. The DS hybridizes with the aptamer in the absence of the target but is displaced by ligand binding as the free target concentration increases. This leads to target-dependent conformational switching of the ISD aptamer, which can be fluorescently measured using a fluorophore-quencher pair coupled to the ends of the construct. However, because the ISD design introduces an intramolecular competitor within the aptamer switch that interferes with binding, the resulting ISD construct will always exhibit reduced affinity and temporal resolution compared to that of the native aptamer. The PANDAS design compensates for this reduced affinity by coupling the ISD aptamer switch to an antibody that recognizes the same target through a different epitope with higher affinity (see Figure S1 for a schematic of the assembly process). The result is a hybrid molecular sensor that achieves high sensitivity through two-epitope binding (Figure 1b). Because the antibody has a higher affinity than the aptamer, the chimeric antibody–aptamer PANDAS construct has a higher probability of target binding at low concentrations than the aptamer alone would. Sensitivity is further enhanced, as

https://doi.org/10.1021/acssensors.3c01638
ACS Sens. XXXX, XXX, XXX−XXX

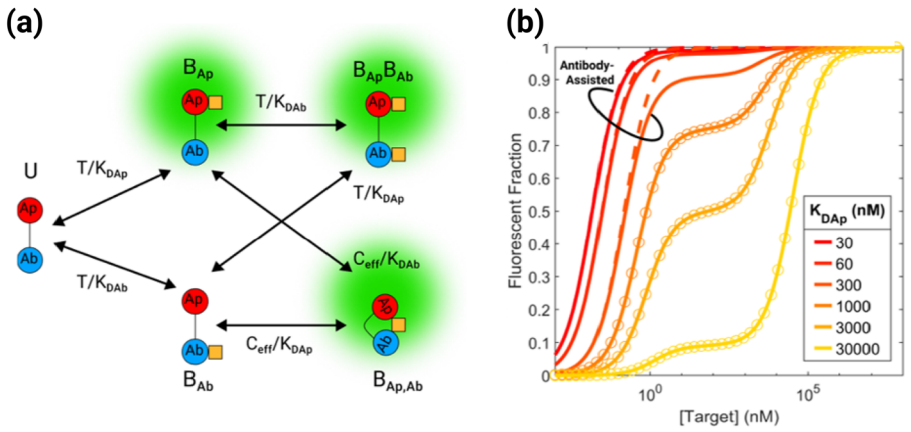

Figure 2. Modeling the thermodynamic binding behavior of the PANDAS construct. (a) Our simplified PANDAS model considers five conformations for the aptamer (Ap), antibody (Ab), and target (yellow square): unbound (U), target singly bound to the aptamer (B_{Ap}) or antibody (B_{Ab}), bivalently bound conformation ($B_{Ap,Ab}$), and doubly bound conformation ($B_{Ap}B_{Ab}$). (b) Tuning of PANDAS affinity by changing ISD aptamer affinity. The plot shows the fraction of fluorescently active constructs at various concentrations of target in a scenario where K_{DAb} = 3 nM, C_{eff} = 3 μM, and K_{DAp} ranges from 30 nM−30 μM. Solid lines represent plots of the full thermodynamic binding model. Dashed lines represent the simplified single-isotherm approximation used for $K_{DAp} \ll C_{eff}$. Circled dot markers represent the dual-isotherm approximation used with $K_{DAp} \geq C_{eff}$.

compared to an aptamer switch alone, by the proximity of the aptamer and antibody such that target binding to one of the receptors increases the effective concentration of target for the other. This leads to a high degree of aptamer binding and fluorescent signaling upon target capture by either the aptamer or the antibody within PANDAS. The ISD design also allows fine-tuning of the aptamer switch function through changes in its DNA sequence. For example, increasing the length of the DS will shift the equilibrium toward the fully folded and quenched state by forming a more stable stem structure.[22] This results in background signal suppression at the expense of a decreased aptamer switch affinity and temporal resolution. Conversely, decreasing the DS length reduces the strength of intramolecular binding competition, thus increasing the aptamer switch affinity and temporal resolution at the cost of a higher background signal.

The antibody component is site-specifically modified with a 30-nt DNA tether at its Fc domain, which is, in turn, tethered to the aptamer switch component via hybridization to a complementary tether sequence that is appended to the fluorophore-tagged DS end of the ISD aptamer (all sequences shown in Table S1). This site-specific tethering ensures reproducible interactions between the target-binding sites of the aptamer and antibody, thereby enabling two-epitope binding and reliable aptamer signaling. The modularity of this design allows for the ready substitution of different aptamer switches or antibody candidates within the PANDAS construct, enabling rapid testing of different switch configurations.

Thermodynamic Modeling of the PANDAS Binding Mechanism. To understand the degree of aptamer affinity enhancement that could be achieved, we developed a thermodynamic model of target-induced binding and switching for the PANDAS construct. We modeled the construct as two linked and noncompeting receptors: the aptamer and the antibody. The binding and switching of the chimeric construct are modeled in terms of target-dependent equilibria among five states, which in turn represent different combinations of target binding for the two receptors (Figure 2a). In the majority of cases, the antibody affinity will be higher than that of the ISD aptamer, such that it will bind with higher probability than the aptamer alone at low target concentrations. The effective concentration of target in the proximity of the ISD aptamer will be dramatically increased due to the aptamer−antibody linkage, and this high effective concentration will ensure a high probability of aptamer binding and fluorescent signaling when the PANDAS construct is in the target-bound state. We assume that the switch produces fluorescent signal only in states where the aptamer is bound to the target. In this model, the function of the PANDAS construct is dictated by three properties of the switch: K_{DAp}, K_{DAb}, and C_{eff}. C_{eff} is the effective concentration of target experienced by the aptamer when the target is already bound to the antibody, while K_{DAp} and K_{DAb} are the equilibrium dissociation constants of the aptamer and antibody, respectively. While K_{DAb} and C_{eff} are not easily tunable within the PANDAS design, the above-mentioned ISD tuning strategy allows us to control K_{DAp}.

We leveraged this model to predict the binding response of the PANDAS construct for different values of K_{DAp} (Figure 2b; see Supplementary Discussion for details). We identified two different binding regimes for the PANDAS construct. The 'antibody-assisted' regime corresponds to values of K_{DAp} where $C_{eff} \gg K_{DAp} \gg K_{DAb}$. In this case, when the target molecule is bound to the antibody, the aptamer binds to it with a high probability and vice versa. As such, the aptamer-bound-only state, B_{Ap}, does not contribute meaningfully to the binding signal, and the fraction of fluorescent constructs is well-approximated by a single isotherm:

$$F(T) \approx \frac{T}{\frac{K_{DAb}K_{DAp}}{2C_{eff}} + T} \quad (1)$$

This approximation is shown as dashed lines in Figure 2b. In the antibody-assisted regime, the PANDAS effective affinity (K_{DEff}) is given by $K_{DAb}K_{DAp}/(2C_{eff})$ and thus depends linearly on the affinity of the ISD aptamer component, scaled by an enhancement factor of $K_{DAb}/(2C_{eff})$. As K_{DAp} approaches or exceeds C_{eff} ($K_{DAp} \geq C_{eff} \gg K_{DAb}$), the B_{Ap} state becomes more prominent, as the PANDAS construct can adopt states where the antibody is target-bound without inducing aptamer binding

https://doi.org/10.1021/acssensors.3c01638
ACS Sens. XXXX, XXX, XXX−XXX

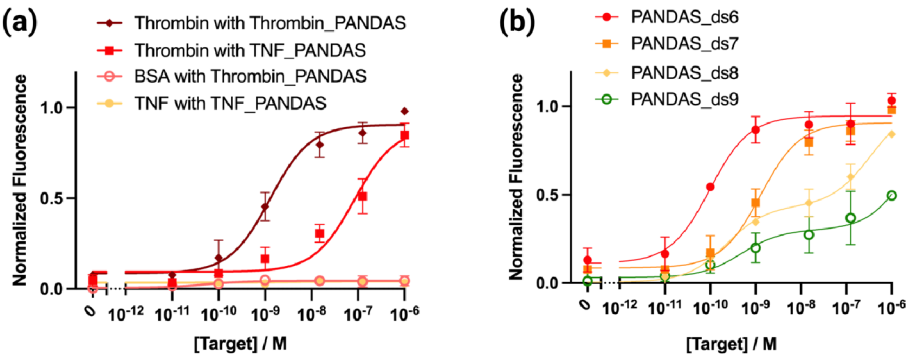

Figure 3. Specificity and tunability of PANDAS constructs. (a) Testing of PANDAS specificity and the impact of two-epitope binding. We used a flow-cytometry-based assay to measure the binding-induced fluorescent readout from our thrombin PANDAS in the presence of thrombin and bovine serum albumin (BSA) compared to a single-epitope-binding PANDAS construct with a mismatched anti-TNF-α antibody exposed to thrombin or TNF-α. (b) Tuning the binding affinity of the thrombin PANDAS construct. We tailored the length of the DS sequence in our PANDAS to range from 6 to 9 nt and then used flow cytometry to measure fluorescence after 30 min of incubation with varying concentrations of thrombin. All data points and error bars represent the mean and standard deviation of three replicates. All curve fitting was applied as described by 'Fitting of Binding Curve Data' within the Methods section.

and vice versa. In these states, the aptamer behaves as a standalone receptor, as no two-epitope binding occurs. In this 'antibody-independent' regime, the fraction of fluorescent PANDAS constructs is better approximated by a dual-isotherm given by

$$F(T) \approx \frac{C_{\mathrm{eff}}}{K_{\mathrm{DAp}} + C_{\mathrm{eff}}} \cdot \frac{T}{\frac{K_{\mathrm{DAb}} K_{\mathrm{DAp}}}{2C_{\mathrm{eff}} + 2K_{\mathrm{DAp}}} + T} + \frac{K_{\mathrm{DAp}}}{K_{\mathrm{DAp}} + C_{\mathrm{eff}}} \cdot \frac{T}{K_{\mathrm{DAp}} + C_{\mathrm{eff}} + T} \quad (2)$$

This approximation is shown in Figure 2b as circled dot symbols. The first high-affinity isotherm describes the antibody-assisted signal, while the latter low-affinity isotherm describes the contribution of the B_{Ap} state. When $K_{DAp} \gg C_{eff}$ (i.e., the aptamer affinity is so low that the proximity of antibody-bound targets is insufficient to trigger aptamer binding), the PANDAS binding response depends only on the affinity of the aptamer. As such, aptamers with extremely low affinities (e.g., in the mM range) will not experience affinity enhancement from a tethered high-affinity antibody, as the local enhancement of the target concentration from proximity will be insufficient to enhance aptamer binding. Fortunately, most protein-binding aptamers exhibit affinities in the submicromolar range and are thus suitable for use in the PANDAS design.

Testing the PANDAS Construct with a Thrombin Model System. As a proof-of-concept demonstration of the affinity and sensitivity enhancement that can be achieved with PANDAS, we designed a fluorescent sensor for thrombin, an important factor in the blood clotting process for which several well-characterized aptamers and monoclonal antibodies have been described.[25−30] Using flow cytometry, we performed pairwise screening of potential aptamer (TBA, HD22) and antibody candidates (5020, F1) to determine an appropriate aptamer−antibody pair and determined that the combination of the 5020 antibody and TBA aptamer achieved the robust sandwich binding of thrombin (Figures S2 and S3). We chose to move forward with testing of the TBA, rather than the higher affinity HD22 aptamer, in order to test our hypothesis that a key advantage of the PANDAS design is the enhancement of sensitivity when using moderately performing aptamer switches for low-abundance protein detection.

We then converted the TBA sequence to an ISD-based fluorescent molecular switch. Initially, we selected a DS length of 7 nucleotides to achieve a high amplitude switching signal with moderate binding affinity. Since the PANDAS enhancement mechanism depends on the affinity difference between the aptamer and antibody, we performed biolayer interferometry (BLI) experiments to determine the affinities of our individual switch components (Figures S4−S6). As expected, our TBA-based ISD aptamer switch exhibited a lower affinity (K_D = 250 nM) compared to the parent aptamer (K_D = 110 nM), whereas the 5020 antibody had a much higher affinity (K_D = 2.8 nM) than the aptamer switch. These results supported the suitability of this affinity reagent pair to achieve enhancement of aptamer binding at low target concentrations based on our two-epitope binding model. We then site-specifically modified 5020 antibody heavy chains at their Fc region with a 30-nt tether oligo at a controlled antibody-to-DNA ratio in order to ensure that each aptamer switch can undergo two-epitope binding with the corresponding antibody Fab region. The efficiency of this conjugation was determined using SDS-PAGE and was found to produce approximately the desired 1:1 antibody-to-DNA conjugation ratio (Figure S7). Subsequently, the TBA ISD aptamer sequence was hybridized to this tether oligo to produce the complete PANDAS construct. The sequences were designed such that the tether between aptamer and antibody consisted of a 30-nt hybridization region as well as a 5-nt single stranded poly-T spacer, such that the overall 35-nt tether region is sufficiently long to achieve robust antibody−aptamer hybridization across long time spans with minimal dissociation, while not being so long that steric interference might impede sandwich binding. The assembled PANDAS construct was then immobilized onto microbeads coated with protein G, which binds to the antibody Fc region. These PANDAS-conjugated beads were incubated for 30 min in buffer spiked with a range of thrombin concentrations, followed by measurement of fluorescent switching using a flow cytometer. As a control, we generated a single-epitope-binding PANDAS construct in which the TBA ISD was coupled to an anti-TNFα antibody that does not bind the thrombin target and challenged this construct with the same range of thrombin concentrations. This assay showed

https://doi.org/10.1021/acssensors.3c01638
ACS Sens. XXXX, XXX, XXX−XXX

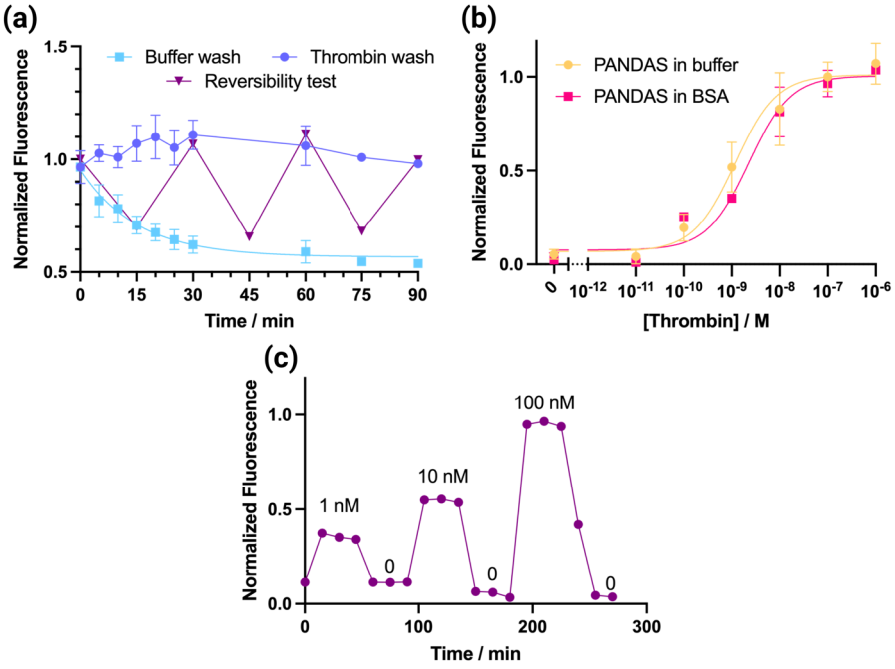

Figure 4. PANDAS kinetics and reversibility of target binding. (a) To measure the kinetics of PANDAS_ds7, we generated dissociation curves by washing thrombin-saturated PANDAS beads with buffer (buffer wash) or 1 μM thrombin (thrombin wash) and measuring fluorescence throughout the dissociation process, to assess reversibility, we transferred PANDAS_ds7-coupled beads between buffer and 1 μM thrombin (reversibility test), collecting fluorescence measurements 15 min after each shift. As controls, we collected fluorescence measurements from PANDAS-ds7 beads that were maintained in either buffer or 1 μM thrombin. (b) PANDAS deployment in an interferent-rich environment. PANDAS_ds7 maintained consistent thrombin-binding performance in buffer alone or containing 530 μM albumin. (c) We also tested the sensor's capacity for continuous sensing of a physiological range of thrombin concentrations in buffer containing 530 μM albumin, with data collected every 15 min. (a) Buffer wash and thrombin wash and (b) data points and error bars respectively represent the mean and standard deviation of three replicates. All curve fitting was applied as described by 'Fitting of Binding Curve Data' within the Methods section.

that our PANDAS construct had a K_D of 1.3 nM (95% confidence interval = 0.8−2.1 nM) and a limit of detection (LOD) of 130 pM (Figure 3a), achieving >50-fold greater affinity and sensitivity relative to the single-epitope-binding control construct (K_D = 83 nM, 95% CI = 32−180 nM; LOD = 8.2 nM). We also ruled out effects of nonspecific protein binding by testing the thrombin antibody-based PANDAS construct against bovine serum albumin (BSA), as well as effects of antibody binding without specific aptamer binding by challenging the anti-TNFα-based PANDAS construct with various concentrations of TNFα, and in both cases we observed no fluorescent signal changes. Notably, TNFα is a target with demonstrated affinity to short, G-quadruplex-based aptamers similar to the TBA used here;[31] thus, the lack of response to TNFα indicates that PANDAS has a strong selectivity even among proteins that are likely to cross-react. These experiments confirmed that signal generation was dependent on aptamer recognition of the target, whereas the affinity and sensitivity increase were contingent upon the specific and two-epitope binding of both antibody and aptamer.

Rational Sequence-Based Tuning of the PANDAS. Building on insights from our thermodynamic model, we developed a range of PANDAS designs in which we tuned the ISD component by extending or shortening the DS. We predicted that elongating the DS would stabilize its hybridization to the aptamer and increase its competition with target binding, thereby decreasing the thrombin affinity of both the aptamer and the overall PANDAS construct. Conversely, shortening the DS should weaken intramolecular competition, leading to higher thrombin affinity for the aptamer and PANDAS. We selected DS lengths ranging from 6 to 9 nt (using the naming convention Aptamer_ds#), immobilized these constructs onto beads, and quantified their thrombin-binding affinity using the flow cytometry-based approach described in section 'Testing the PANDAS Construct with a Thrombin Model System'.

As expected, decreasing the DS length increased ISD aptamer binding affinity and thus shifted the dynamic range for higher sensitivity toward lower target concentrations (Figure S8). For example, decreasing the DS length from 7 to 6 nt led to a decrease in K_D from 95 (95% CI = 62−150 nM) to 30 nM (95% CI = 20−46 nM). Conversely, extending the DS length from 7 to 9 nt weakened the aptamer's sensitivity considerably, yielding binding curves for which it proved difficult to achieve saturation and an affinity >500 nM for the 9-nt design (95% CI = 260−1.1 μM). We next assembled these ISD constructs into full PANDAS constructs with the antithrombin antibody and again assessed their binding via flow cytometry (Figure 3b). Between PANDAS_ds6 and PANDAS_ds9 and taking into account both antibody-assisted and antibody-independent aptamer signaling, we observed a range of switch affinities spanning from ∼100 pM to ∼1 μM. These experimentally derived binding curves aligned quite well with the two binding regimes predicted by our model. The binding of PANDAS_ds6 and PANDAS_ds7 is well approximated by single-isotherm binding owing to antibody-assisted binding with increased affinity and sensitivity. These PANDAS_ds6 and PANDAS_ds7 designs achieved K_D values of 98 pM (95% CI = 58−170 pM) and 1.3 nM (95%

https://doi.org/10.1021/acssensors.3c01638
ACS Sens. XXXX, XXX, XXX−XXX

CI = 0.8−2.1 nM) and LOD values of 16 pM and 130 pM, respectively. Thus, compared to the aptamer-only sensor, our highest-sensitivity PANDAS design achieves a >300-fold enhancement of both affinity and LOD. In contrast, PANDAS_ds8 and PANDAS_ds9 exhibited two-stage binding due to antibody-independent binding. Thus, these designs offer a broader dynamic range, spanning from subnanomolar LOD's to saturation at concentrations greater than 1 μM. The ability to rationally tune the PANDAS response to achieve either high sensitivity or wide dynamic range offers the potential for optimization toward specific biomolecular detection applications. Although PANDAS_ds6 exhibited the best sensitivity, its background was also high due to the reduced stability of DS hybridization. For the remainder of this work, we chose PANDAS_ds7 for further characterization because of its low background, high signal gain, and relatively high thrombin sensitivity.

To evaluate the kinetic response of this construct, we dispensed PANDAS_ds7-coupled beads into a 1 μM thrombin-spiked buffer and incubated them for three min to allow them to equilibrate. We then washed the beads with thrombin-free buffer and periodically interrogated the PANDAS fluorescent binding response via flow cytometry to observe the target dissociation signal (Figure 4a, buffer wash and thrombin wash). As a control, we repeated this experiment by washing the beads with the same 1 μM thrombin-containing solution, which should result in minimal dissociation. We measured a dissociation rate of k_{off} = 1.1 × 10^{-3} s^{-1}, which indicates that the PANDAS construct maintains a reasonable off-rate that is suitable for tracking endogenous target concentration changes in continuous sensing applications given an antibody with typical binding kinetics. We also evaluated the reversibility of binding by deploying the PANDAS-coupled beads into alternating solutions of 1 μM thrombin and buffer, incubating for 15 min each time, and then interrogating the construct via flow cytometry (Figure 4a, reversibility test). The PANDAS receptor was able to track these changes in concentration over many cycles, with the binding signal returning to near-baseline levels every time.

Finally, we assessed the PANDAS construct's performance as a continuous sensor in complex samples. Working with the protein-rich matrix of blood, serum, or plasma would have required a careful selection of samples to avoid the influence of proteins that interferes with our ability to accurately measure spiked-in thrombin concentrations. Endogenous antithrombin III (ATIII), heparin cofactor II (HCII), and alpha-2-macroglobulin (A2M) can all form complexes with thrombin and thereby interfere with the function of our PANDAS sensor.[32−34] We therefore used a surrogate protein-rich biofluid of defined content, challenging our switch with buffer containing physiologically representative concentrations of BSA (~530 μM) as a surrogate for human albumin—a large protein that is prone to nonspecific binding and composes 60% of total plasma protein content.[35] We measured the fluorescent response of PANDAS_ds7 in this albumin-rich solution using the same bead-based fluorescent assay described above, with 30 min sample incubation time. The affinity for thrombin in the presence of albumin did not differ significantly from buffer, and the limit of detection was only slightly increased (Figure 4c), with the sensor exhibiting K_D = 2.3 nM (95% CI = 1.3−4.1 nM) and LOD = 260 pM (as compared to K_D = 1.3 nM, 95% CI = 0.8−2.1 nM, LOD = 130 pM in buffer). This is especially notable as the TBA aptamer has been reported to cross-react with BSA with micromolar affinity.[36] To further investigate the PANDAS function in blood-derived complex fluids, we applied 50 kDa filter to diluted human blood in order to remove confounding proteins (e.g., antithrombin is >50 kDa) while maintaining its complex ionic, small molecule, and small protein/peptide content. Upon testing in this sample, the PANDAS construct retains its target-sensing capabilities (Figure S9) and achieves a sensitivity to low thrombin concentrations similar to its performance in buffer in the low concentration range (LOD = 41 pM in filtered blood). Notably, we do observe that the construct exhibits two-stage binding at concentrations >1 nM, suggesting a mixture of antibody-assisted and antibody-independent binding. According to our mechanistic PANDAS model, this may result from slightly diminished aptamer affinity and may indicate that the slightly different ionic or small molecule content of blood diminishes the aptamer affinity somewhat. However, this also shows that even with slightly diminished aptamer affinity, the strength of antibody-assisted binding allows for sensitive detection at low thrombin concentrations. While this sample has lower protein content than whole blood, it is still promising for human applications as this lower-protein content fluid is representative of interstitial fluid or sampling obtained through tissue microdialysis. Taken together, these results in high BSA protein content and filtered blood indicate that the PANDAS design can leverage the antibody's excellent specificity to facilitate sensitive aptamer-based detection in complex samples. Finally, to test our construct's capacity for time-resolved continuous sensing in complex samples, we sequentially incubated our beads with varying physiological-range concentrations of thrombin in the presence of 530 μM albumin and measured the switch response every 15 min (Figure 4d). We observed stable concentration-dependent measurements over the entire 270 min experiment, demonstrating the potential for continuous monitoring of analyte concentrations with our PANDAS receptor.

CONCLUSIONS

Molecular switches are valuable tools for the rapid detection and continuous monitoring of diverse analytes, but existing approaches for generating such reagents suffer from notable limitations. Aptamer-based switches such as aptamer beacons and the ISD constructs used in this work can be relatively straightforward to engineer from existing aptamers, but the engineering process tends to sacrifice the sensitivity of the final molecular switch. In contrast, antibodies generally offer excellent affinity and specificity in the context of end point-based measurements, even in complex samples, but it remains challenging to achieve continuous analyte detection using antibody-based assays beyond a handful of preliminary demonstrations.[10,37,38] Our PANDAS design combines the desirable properties of both types of receptor—enhancing the affinity and specificity of an ISD-based aptamer switch by linking it to a target-specific antibody. In this design, the antibody's high-affinity binding and the high effective concentration between the aptamer and antibody lead to enhanced two-epitope binding. The aptamer produces a fluorescent readout for sensing and can readily be tuned by modulating the ISD design to optimize its sensitivity. Using thrombin as a model analyte, we demonstrated that the PANDAS design can enhance the affinity and sensitivity of protein detection by >300-fold relative to the ISD-based aptamer switch on its own. The resulting PANDAS are highly

https://doi.org/10.1021/acssensors.3c01638
ACS Sens. XXXX, XXX, XXX−XXX

analyte-specific, leveraging two-site binding from both elements to recognize their target with high sensitivity. We show that the PANDAS design can achieve rapid and reversible switching over multiple cycles of target binding and washing, suggesting the feasibility of applying these receptors toward continuous detection with minute-scale temporal resolution. We also demonstrate the ability to monitor fluctuating levels of thrombin within a physiological concentration range in complex samples containing high levels of interferent protein. While this initial demonstration focuses only on the detection of thrombin, this approach should be compatible with aptamer switches developed through a wide range of approaches, as long as an antibody that binds to a separate, noncompeting epitope can be used. The breadth of commercially available antibodies should ensure that a two-epitope binding antibody−aptamer pair can be obtained for most or all protein targets. While the design of new structure switching aptamers is not trivial, emerging work is enhancing the design of such switches either through rational design to induce and tune aptamer structure switching,[21,22,39] or the use of high-throughput combinatorial screening to directly isolate such switches.[40] Thus, the PANDAS design offers the potential to enhance the sensitivity of sensors for a variety of lower-abundance biomarkers.

It should be noted that this is only an initial demonstration of the PANDAS concept, and additional work will be needed to maximize the utility of this reagent design. As the design is extended to more protein biomarkers, the aptamer function must be carefully optimized to ensure both high sensitivity and suitable temporal resolution of measurements. The PANDAS construct's dissociation rate will generally be bounded by the antibody's binding affinity, and any affinity increases from two-epitope binding should only serve to decrease the dissociation rate. As such, rapid measurements at subnanomolar concentrations pose a substantial technical challenge. That being said, we do see other avenues for achieving improved temporal resolution. Moderate-affinity antibodies (low nanomolar K_D) exhibit higher dissociation rates on the order of 10^{-4} to 10^{-3} s^{-1}, which corresponds to an equilibration time of approximately 15−150 min.[41] This still poses a substantial time delay for equilibration, but emerging 'pre-equilibrium' measurement methods may offer a route to surpass these time scales. We recently described one such approach, in which we extract the kinetic information from affinity sensor responses during the equilibration period rather than waiting for arrival at the equilibrium.[42,43] Thus, we believe that combining pre-equilibrium measurements with a PANDAS design leveraging an antibody with a fast dissociation rate may provide a path for using this PANDAS construct to sense subnanomolar targets with response times on the order of tens of minutes. In this demonstration, we have made use of flow cytometry to demonstrate the reversibility and minute-scale measurement kinetics of the PANDAS fluorescent target-binding response. However, achieving continuous real-time sensing that is compatible with wearable or field applications will require a more sophisticated sensor design that enables surface-based fluorescent measurements with high temporal resolution in a sensor format that is less complex than cytometry and does not require continuous flow. Fortunately, emerging optical fiber-based fluorescent sensors have been demonstrated to be capable of continuous molecular switch-based measurement in biofluids and rely on fluorescent wavelengths and surface chemistries that should be highly compatible with our PANDAS design with minimal modification.[20] Such surface-based sensors will also enable further investigation of the quantitative performance of PANDAS-based measurements in more complex biological specimens. Although we were able to show that the sensing performance was unimpeded by high background levels of interferent protein, it remains to be seen whether this system will remain equally robust in the context of blood and other complex biological matrices that are incompatible with bead-based assays. Overall, we see considerable future potential for this sensor design approach, which we believe should be broadly generalizable across a range of molecular targets and offer the opportunity to convert moderate-quality aptamers into highly useful reagents for achieving sensitive molecular detection in interferent-rich specimens.

METHODS

Reagents and Materials. DNA oligonucleotides with fluorophore-quencher modifications were purchased from Integrated DNA Technologies. All sequences are shown in Table S1. Unless otherwise specified, all other reagents were ordered from Thermo Fisher Scientific. Oligonucleotide concentrations were determined by UV spectroscopy using a Nanodrop ND2000 spectrophotometer. Thrombin (HCT-0020 human α-thrombin) was purchased from Haematologic Technologies. Thrombin monoclonal antibody 5020 (catalog no. MA1-43019) was purchased from Thermo Fisher Scientific. Thrombin monoclonal antibody F1 (sc-271449) was purchased from Santa Cruz Biotechnology. TNF-α antibody was purchased from Biolegend (catalog # 502802). Molecular biology grade BSA was purchased from New England Biolabs. Protein G Dynabeads (catalog no. 10-004-D) were purchased from Invitrogen. PBS, Salmon Sperm DNA, goat IgG, EDTA, NuPAGE sample reducing agent, NuPAGE LDS sample buffer (4×), NuPAGE 4 to 12% Bis-Tris mini protein gels, 20× NuPAGE MES SDS running buffer, SeeBlue prestained protein standard, SimplyBlue SafeStain, UltraPure TBE buffer (10×), Novex TBE-Urea Gels (10%), GelStar nucleic acid gel stain, and Tween 20 were purchased from Thermo Fisher Scientific.

Screening Aptamer−Antibody Pairs for the PANDAS Construct. We tested two Cy5-labeled thrombin aptamer sequences (TBA and HD22) and two different antithrombin antibodies (5020 and F1). 200 nM antibody was incubated with 10 μL of protein G Dynabeads in 50 μL of 1 × ISD binding buffer (10 mM Tris−HCl, pH 7.5 and 6 mM $MgCl_2$) for 30 min at room temperature. The beads were washed three times to remove any nonspecific bindingand then incubated with 450 nM aptamer in the presence or absence of 300 nM thrombin in a final volume of 50 μL ISD buffer for 30 min at room temperature.

PANDAS Assembly. We used the SiteClick antibody azido modification kit (S20026, Thermo Fisher Scientific) to modify the antibody Fc region in a site-specific fashion. 100 μg of antibody was treated with 10 μL of β-galactosidase in 20 μL of 1× PBS buffer at 37 °C overnight to remove the terminal β-D-galactoside. The uncapped antibodies were then treated with 80 μL of GalT transferase and UDP-GalNAz in 1× Tris buffer at 30 °C overnight to add azide caps. 50K Amicon purification columns were used to remove excessive UDP-GalNAz. 50 μL of 100 μM amine-modified tether oligonucleotides (Ab2-tether) was treated with 100 μL of 17 mM DBCO-NHS at room temperature overnight to equip these oligos with DBCO

https://doi.org/10.1021/acssensors.3c01638
ACS Sens. XXXX, XXX, XXX−XXX

moieties. The oligos were then ethanol precipitated to remove excess reactants and resuspended in 1× ISD buffer. 10 μL of 100 μM DBCO-modified tether oligonucleotides was reacted with 10 μL of 10 μM azido-antibody in 1× PBS buffer, and the degree of antibody labeling was determined by running a reducing NuPAGE gel (see section 'Antibody Labeling Quantification in Reducing Gels'). The antibody-tether complexes were stored at 4 °C until further use. To make fresh PANDAS, 2 μL of 5 μM antibody-tether complexes was hybridized to 1 μL of 100 μM aptamers in hybridization buffer (1× PBS, 1 mg/mL BSA, 0.05% Tween 20, 15 μg/m goat IgG, 0.1 mg/mL salmon sperm DNA, and 5 mM EDTA) overnight. 10 pmol of PANDAS chimera was then captured by 10 μL of prewashed protein G Dynabeads and washed three times with ISD buffer to remove excess aptamers.

Antibody Labeling Quantification in Reducing Gels. We quantified the degree of antibody oligo labeling with a 10% NuPAGE gel. 1 μL of NuPAGE reducing reagent was incubated with 12 pmol of unmodified antibody or click-modified antibody in a total volume of 10 μL of 1× NuPAGE sample loading buffer at 95 °C for 5 min. The samples were then quickly loaded onto the 10% Bis-Tris mini protein gel and run at 200 V for 30 min. After 30 min, the gel was transferred to 100 mL of SimplyBlue SafeStain staining solution for another 30 min. The gel was rinsed with water twice to destain before imaging on a ChemiDoc MP System (Bio-Rad Laboratories).

Biolayer Interferometry (BLI) Analysis of PANDAS Components. BLI affinity measurements were done on an Octet Red 96 instrument (Pall ForteBio), with streptavidin sensors (SA, Sartorius) and Fc capture sensors (AMC, Sartorius). Sensors were prehydrated in ISD buffer for at least 20 min before use. 200 μL of 20 nM biotinylated aptamers or antibodies in ISD buffer was used for ligand loading to reach ∼0.5 nm loading levels. After ligand loading, sensors were dipped in ISD binding buffer containing various thrombin concentrations (25, 50, 100, or 200 nM for aptamer measurements; 10, 20, 40, or 80 nM for antibody measurements) for 300 s and then dipped in ISD buffer for 600 s. To avoid nonspecific binding, every thrombin concentration was measured with both assay and reference sensors. Final signals were processed via subtraction from the reference sensors.

Measurements of Effective Binding Affinity. To obtain binding curves, 50 μL of reaction volume was prepared in 1× ISD binding buffer with 10 nM PANDAS-coupled beads and thrombin concentrations in the range of 1 nM−1 μM and was incubated for 30 min at room temperature. For ISD-only tuning experiments, we used a TNF-α antibody that was shown to have no affinity for thrombin as a dummy antibody in the final PANDAS construct. For baseline determination with the PANDAS alone, 50 μL of 10 nM PANDAS-coupled beads was prepared in ISD binding buffer without thrombin. The mean fluorescence intensities for all samples were measured at 25 °C on a flow cytometer (BD Accuri C6 Plus). Representative scatter plots, histograms, and strategies used for gating to extract singlet bead populations from flow cytometry are shown in Figure S9. All samples were prepared and analyzed in triplicate.

For the reversibility experiments, three samples of 10 nM PANDAS-coupled beads and 1 μM thrombin in 50 μL of 1× ISD buffer were incubated for 30 min at room temperature to reach saturation. The sample tubes were then put in a magnetic rack (Life Technologies) for 2 min to separate the PANDAS beads and sample liquid. For the first sample, we maintained saturation with 50 μL of 1 μM thrombin in ISD buffer added to the beads every 15 min. The second sample was for reversibility testing, and 50 μL of ISD buffer or 1 μM thrombin in ISD buffer was added every 15 min in an alternating fashion. The third sample was used to measure dissociation only with 50 μL of 1× ISD binding added to the PANDAS beads every 15 min. The mean fluorescence intensities for all samples were measured at 25 °C on a flow cytometer.

Fitting of Binding Curve Data. We applied a single-site langmuir isotherm binding model to fit and normalize ISD data and PANDAS_ds6 and _ds7 data from the flow cytometer for ease of comparison:

$$y = (B_{max} - y_0)\frac{x}{x + K_D^{eff}} + y_0 \quad (3)$$

We applied a two-site binding model to fit pre-normalized (to the highest measured value within the dataset) PANDAS_ds8 and _9 data from the flow cytometer as these data exhibit a combination of antibody-assisted and antibody-independent binding:

$$y = (B_{max}\mathrm{Hi})\frac{x}{x + K_D^{Hi}} + (1 - B_{max}\mathrm{Hi} - y_0)\frac{x}{x + K_D^{Lo}} + y_0 \quad (4)$$

These two fitting models (one- and two-site) were motivated by our theoretical analysis of the PANDAS binding behavior presented in the main text and summarized in Equation 1 and Equation 2. The average fluorescence value from three replicates was divided by B_{max} before plotting of the single-site binding curve data. Error bars were calculated as propagation of errors for standard deviation from the average fluorescence and error in the fit for B_{max}.

LODs were determined from the mean values of B_{max}, y_0, and as determined from fitting, as well as the standard deviations (σ) of these parameters. We applied the standard definition of LOD, which is the target concentration at which the fluorescent response is three standard deviations above background. Thus, LODs for all constructs were determined by solving the equation:

$$3\sigma_{y_0} = B_{max}\frac{\mathrm{LOD}}{K_D^{eff} + \mathrm{LOD}} \quad (5)$$

■ ASSOCIATED CONTENT

Data Availability Statement

This work has been deposited on bioRxiv prior to publication in ACS Sensors, where it is available at: 10.1101/2023.08.08.552518.

Supporting Information

The Supporting Information is available free of charge at https://pubs.acs.org/doi/10.1021/acssensors.3c01638.

Detailed sequences of all DNA oligos used in project, schematics for PANDAS construct synthesis, flow cytometry data supporting aptamer−antibody sandwich capability, BLI measurement data for aptamers and antibodies used, gel electrophoresis assessment of antibody−DNA conjugation, ISD aptamer tuning data, flow cytometry data for PANDAS performance in filtered human blood, and detailed discussion of the

https://doi.org/10.1021/acssensors.3c01638
ACS Sens. XXXX, XXX, XXX−XXX

thermodynamic binding model for the PANDAS construct (PDF)

AUTHOR INFORMATION

Corresponding Author

Hyongsok Tom Soh − *Department of Radiology, Stanford University, Stanford, California 94305, United States; Department of Electrical Engineering, Stanford University, Stanford, California 94305, United States;* orcid.org/0000-0001-9443-857X; Email: tsoh@stanford.edu

Authors

Dehui Kong − *Department of Radiology, Stanford University, Stanford, California 94305, United States;* orcid.org/0000-0002-5906-8814

Ian A. P. Thompson − *Department of Electrical Engineering, Stanford University, Stanford, California 94305, United States*

Nicolo Maganzini − *Department of Electrical Engineering, Stanford University, Stanford, California 94305, United States*

Michael Eisenstein − *Department of Radiology, Stanford University, Stanford, California 94305, United States; Department of Electrical Engineering, Stanford University, Stanford, California 94305, United States*

Complete contact information is available at: https://pubs.acs.org/10.1021/acssensors.3c01638

Author Contributions

#D.K., I.A.P.T., and N.M. contributed equally.

Notes

The authors declare no competing financial interest.

ACKNOWLEDGMENTS

H.T.S. gratefully acknowledges financial supported by Helmsley Charitable Trust, the Stanford Maternal and Child Health Research Institute (MCHRI) and the Wellcome LEAP SAVE program. I.A.P.T. was supported by the Medtronic Foundation Stanford Graduate Fellowship and the Natural Sciences and Engineering Research Council of Canada (NSERC, 416353855).

REFERENCES

(1) Kumar, A.; Roberts, D.; Wood, K. E.; Light, B.; Parrillo, J. E.; Sharma, S.; Suppes, R.; Feinstein, D.; Zanotti, S.; Taiberg, L.; Gurka, D.; Kumar, A.; Cheang, M. Duration of Hypotension before Initiation of Effective Antimicrobial Therapy Is the Critical Determinant of Survival in Human Septic Shock. *Crit. Care Med.* **2006**, *34* (6), 1589−1596.

(2) Keller, T.; Zeller, T.; Peetz, D.; Tzikas, S.; Roth, A.; Czyz, E.; Bickel, C.; Baldus, S.; Warnholtz, A.; Fröhlich, M.; Sinning, C. R.; Eleftheriadis, M. S.; Wild, P. S.; Schnabel, R. B.; Lubos, E.; Jachmann, N.; Genth-Zotz, S.; Post, F.; Nicaud, V.; Tiret, L.; Lackner, K. J.; Münzel, T. F.; Blankenberg, S. Sensitive Troponin I Assay in Early Diagnosis of Acute Myocardial Infarction. *N. Engl. J. Med.* **2009**, *361* (9), 868−877.

(3) Vettoretti, M.; Cappon, G.; Acciaroli, G.; Facchinetti, A.; Sparacino, G. Continuous Glucose Monitoring: Current Use in Diabetes Management and Possible Future Applications. *J. Diabetes Sci. Technol.* **2018**, *12* (5), 1064−1071.

(4) Hellhammer, D. H.; Wüst, S.; Kudielka, B. M. Salivary Cortisol as a Biomarker in Stress Research. *Psychoneuroendocrinology* **2009**, *34* (2), 163−171.

(5) Bhake, R. C.; Kluckner, V.; Stassen, H.; Russell, G. M.; Leendertz, J.; Stevens, K.; Linthorst, A. C. E.; Lightman, S. L. Continuous Free Cortisol Profiles—Circadian Rhythms in Healthy Men. *J. Clin. Endocrinol. Metab.* **2019**, *104* (12), 5935−5947.

(6) Gruenewald, T. L.; Seeman, T. E.; Ryff, C. D.; Karlamangla, A. S.; Singer, B. H. Combinations of Biomarkers Predictive of Later Life Mortality. *Proc. Natl. Acad. Sci. U. S. A.* **2006**, *103* (38), 14158−14163.

(7) Kim, J.; Campbell, A. S.; de Ávila, B. E.-F.; Wang, J. Wearable Biosensors for Healthcare Monitoring. *Nat. Biotechnol.* **2019**, *37* (4), 389−406.

(8) Aydin, S. A Short History, Principles, and Types of ELISA, and Our Laboratory Experience with Peptide/Protein Analyses Using ELISA. *Peptides* **2015**, *72*, 4−15.

(9) Wu, C.; Dougan, T. J.; Walt, D. R. High-Throughput, High-Multiplex Digital Protein Detection with Attomolar Sensitivity. *ACS Nano* **2022**, *16* (1), 1025−1035.

(10) Das, J.; Gomis, S.; Chen, J. B.; Yousefi, H.; Ahmed, S.; Mahmud, A.; Zhou, W.; Sargent, E. H.; Kelley, S. O. Reagentless Biomolecular Analysis Using a Molecular Pendulum. *Nat. Chem.* **2021**, *13* (5), 428−434.

(11) Xiao, Y.; Lubin, A. A.; Heeger, A. J.; Plaxco, K. W. Label-Free Electronic Detection of Thrombin in Blood Serum by Using an Aptamer-Based Sensor. *Angew. Chem. Int. Ed.* **2005**, *44* (34), 5456−5459.

(12) Swensen, J. S.; Xiao, Y.; Ferguson, B. S.; Lubin, A. A.; Lai, R. Y.; Heeger, A. J.; Plaxco, K. W.; Soh, H. T. Continuous, Real-Time Monitoring of Cocaine in Undiluted Blood Serum via a Microfluidic, Electrochemical Aptamer-Based Sensor. *J. Am. Chem. Soc.* **2009**, *131* (12), 4262−4266.

(13) Ferguson, B. S.; Hoggarth, D. A.; Maliniak, D.; Ploense, K.; White, R. J.; Woodward, N.; Hsieh, K.; Bonham, A. J.; Eisenstein, M.; Kippin, T. E.; Plaxco, K. W.; Soh, H. T. Real-Time, Aptamer-Based Tracking of Circulating Therapeutic Agents in Living Animals. *Sci. Transl. Med.* **2013**, *5* (213), 213ra165−213ra165.

(14) Nakatsuka, N.; Yang, K.-A.; Abendroth, J. M.; Cheung, K. M.; Xu, X.; Yang, H.; Zhao, C.; Zhu, B.; Rim, Y. S.; Yang, Y.; Weiss, P. S.; Stojanović, M. N.; Andrews, A. M. Aptamer−field-effect transistors overcome Debye length limitations for small-molecule sensing. *Science* **2018**, *362* (6412), 319−324.

(15) Dauphin-Ducharme, P.; Yang, K.; Arroyo-Currás, N.; Ploense, K. L.; Zhang, Y.; Gerson, J.; Kurnik, M.; Kippin, T. E.; Stojanovic, M. N.; Plaxco, K. W. Electrochemical Aptamer-Based Sensors for Improved Therapeutic Drug Monitoring and High-Precision, Feedback-Controlled Drug Delivery. *ACS Sens.* **2019**, *4* (10), 2832−2837.

(16) Hamaguchi, N.; Ellington, A.; Stanton, M. Aptamer Beacons for the Direct Detection of Proteins. *Anal. Biochem.* **2001**, *294* (2), 126−131.

(17) Li, J. J.; Fang, X.; Tan, W. Molecular Aptamer Beacons for Real-Time Protein Recognition. *Biochem. Biophys. Res. Commun.* **2002**, *292* (1), 31−40.

(18) Moutsiopoulou, A.; Broyles, D.; Dikici, E.; Daunert, S.; Deo, S. K. Molecular Aptamer Beacons and Their Applications in Sensing, Imaging, and Diagnostics. *Small* **2019**, *15* (35), 1902248.

(19) Giannetti, A.; Tombelli, S. Aptamer Optical Switches: From Biosensing to Intracellular Sensing. *Sens. Actuators Rep.* **2021**, *3*, 100030.

(20) Hariri, A. A.; Cartwright, A. P.; Dory, C.; Gidi, Y.; Yee, S.; Fu, K. X.; Yang, K.; Wu, D.; Thompson, I. A. P.; Maganzini, N.; Feagin, T.; Young, B. E.; Afshar, B. H.; Eisenstein, M.; Digonnet, M.; Vuckovic, J.; Soh, H. T. Continuous Optical Detection of Small-Molecule Analytes in Complex Biomatrices. *bioRxiv* **2023**.

(21) Tang, Z.; Mallikaratchy, P.; Yang, R.; Kim, Y.; Zhu, Z.; Wang, H.; Tan, W. Aptamer Switch Probe Based on Intramolecular Displacement. *J. Am. Chem. Soc.* **2008**, *130* (34), 11268−11269.

(22) Wilson, B. D.; Hariri, A. A.; Thompson, I. A. P.; Eisenstein, M.; Soh, H. T. Independent Control of the Thermodynamic and Kinetic Properties of Aptamer Switches. *Nat. Commun.* **2019**, *10* (1), 5079.

(23) Munzar, J. D.; Ng, A.; Juncker, D. Duplexed Aptamers: History, Design, Theory, and Application to Biosensing. *Chem. Soc. Rev.* **2019**, *48*, 1390.
(24) Liu, T.; Qian, W.-J.; Gritsenko, M. A.; Xiao, W.; Moldawer, L. L.; Kaushal, A.; Monroe, M. E.; Varnum, S. M.; Moore, R. J.; Purvine, S. O.; Maier, R. V.; Davis, R. W.; Tompkins, R. G.; Camp, D. G.; Smith, R. D. High Dynamic Range Characterization of the Trauma Patient Plasma Proteome*. *Mol. Cell Proteomics* **2006**, *5* (10), 1899−1913.
(25) Tasset, D. M.; Kubik, M. F.; Steiner, W. Oligonucleotide Inhibitors of Human Thrombin That Bind Distinct Epitopes. *J. Mol. Biol.* **1997**, *272* (5), 688−698.
(26) Bock, L. C.; Griffin, L. C.; Latham, J. A.; Vermaas, E. H.; Toole, J. J. Selection of Single-Stranded DNA Molecules That Bind and Inhibit Human Thrombin. *Nature* **1992**, *355* (6360), 564−566.
(27) Kong, D.; Lei, Y.; Yeung, W.; Hili, R. Enzymatic Synthesis of Sequence-Defined Synthetic Nucleic Acid Polymers with Diverse Functional Groups. *Angew. Chem.* **2016**, *128* (42), 13358−13362.
(28) Kong, D.; Yeung, W.; Hili, R. In Vitro Selection of Diversely Functionalized Aptamers. *J. Am. Chem. Soc.* **2017**, *139* (40), 13977−13980.
(29) Prager, N. A.; Abendschein, D. R.; McKenzie, C. R.; Eisenberg, P. R. Role of Thrombin Compared with Factor Xa in the Procoagulant Activity of Whole Blood Clots. *Circulation* **1995**, *92* (4), 962−967.
(30) Estevez, B.; Kim, K.; Delaney, M. K.; Stojanovic-Terpo, A.; Shen, B.; Ruan, C.; Cho, J.; Ruggeri, Z. M.; Du, X. Signaling-Mediated Cooperativity between Glycoprotein Ib-IX and Protease-Activated Receptors in Thrombin-Induced Platelet Activation. *Blood* **2016**, *127* (5), 626−636.
(31) Orava, E. W.; Jarvik, N.; Shek, Y. L.; Sidhu, S. S.; Gariepy, J. A Short DNA Aptamer That Recognizes TNFα and Blocks Its Activity *in Vitro*. *ACS Chem. Biol.* **2013**, *8* (1), 170−178.
(32) Olson, S. T.; Chuang, Y.-J. Heparin Activates Antithrombin Anticoagulant Function by Generating New Interaction Sites (Exosites) for Blood Clotting Proteinases. *Trends Cardiovasc. Med.* **2002**, *12* (8), 331−338.
(33) Tollefsen, D. M. Heparin Cofactor II Modulates the Response to Vascular Injury. *Arterioscler. Thromb. Vasc. Biol.* **2007**, *27* (3), 454−460.
(34) Straight, D. L.; McKee, P. A. Characterization of Thrombin Binding to Alpha 2-Macroglobulin. *J. Biol. Chem.* **1984**, *259* (2), 1272−1278.
(35) He, X. M.; Carter, D. C. Atomic Structure and Chemistry of Human Serum Albumin. *Nature* **1992**, *358* (6383), 209−215.
(36) Trapaidze, A.; Hérault, J.-P.; Herbert, J.-M.; Bancaud, A.; Gué, A.-M. Investigation of the Selectivity of Thrombin-Binding Aptamers for Thrombin Titration in Murine Plasma. *Biosens. Bioelectron.* **2016**, *78*, 58−66.
(37) Zargartalebi, H.; Yousefi, H.; Flynn, C. D.; Gomis, S.; Das, J.; Young, T. L.; Chien, E.; Mubareka, S.; McGeer, A.; Wang, H.; Sargent, E. H.; Nezhad, A. S.; Kelley, S. O. Capillary-Assisted Molecular Pendulum Bioanalysis. *J. Am. Chem. Soc.* **2022**, *144* (40), 18338−18349.
(38) Thompson, I. A. P.; Saunders, J.; Zheng, L.; Hariri, A. A.; Maganzini, N.; Cartwright, A. P.; Pan, J.; Yee, S.; Dory, C.; Eisenstein, M.; Vuckovic, J.; Soh, H. T. An Antibody-Based Molecular Switch for Continuous Small-Molecule Biosensing. *Sci. Adv.* **2023**, *9* (38), No. eadh4978.
(39) Ricci, F.; Vallée-Bélisle, A.; Simon, A. J.; Porchetta, A.; Plaxco, K. W. Using Nature's "Tricks" To Rationally Tune the Binding Properties of Biomolecular Receptors. *Acc. Chem. Res.* **2016**, *49* (9), 1884−1892.
(40) Yoshikawa, A. M.; Rangel, A. E.; Zheng, L.; Wan, L.; Hein, L. A.; Hariri, A. A.; Eisenstein, M.; Soh, H. T. A Massively Parallel Screening Platform for Converting Aptamers into Molecular Switches. *Nat. Commun.* **2023**, *14* (1), 2336.
(41) Jones, B. E.; Brown-Augsburger, P. L.; Corbett, K. S.; Westendorf, K.; Davies, J.; Cujec, T. P.; Wiethoff, C. M.; Blackbourne, J. L.; Heinz, B. A.; Foster, D.; Higgs, R. E.; Balasubramaniam, D.; Wang, L.; Zhang, Y.; Yang, E. S.; Bidshahri, R.; Kraft, L.; Hwang, Y.; Žentelis, S.; Jepson, K. R.; Goya, R.; Smith, M. A.; Collins, D. W.; Hinshaw, S. J.; Tycho, S. A.; Pellacani, D.; Xiang, P.; Muthuraman, K.; Sobhanifar, S.; Piper, M. H.; Triana, F. J.; Hendle, J.; Pustilnik, A.; Adams, A. C.; Berens, S. J.; Baric, R. S.; Martinez, D. R.; Cross, R. W.; Geisbert, T. W.; Borisevich, V.; Abiona, O.; Belli, H. M.; de Vries, M.; Mohamed, A.; Dittmann, M.; Samanovic, M. I.; Mulligan, M. J.; Goldsmith, J. A.; Hsieh, C.-L.; Johnson, N. V.; Wrapp, D.; McLellan, J. S.; Barnhart, B. C.; Graham, B. S.; Mascola, J. R.; Hansen, C. L.; Falconer, E. The Neutralizing Antibody, LY-CoV555, Protects against SARS-CoV-2 Infection in Nonhuman Primates. *Sci. Transl. Med.* **2021**, *13* (593), No. eabf1906.
(42) Maganzini, N.; Thompson, I.; Wilson, B.; Soh, H. T. Pre-Equilibrium Biosensors as an Approach towards Rapid and Continuous Molecular Measurements. *Nat. Commun.* **2022**, *13* (1), 7072.
(43) Lubken, R. M.; de Jong, A. M.; Prins, M. W. J. Real-Time Monitoring of Biomolecules: Dynamic Response Limits of Affinity-Based Sensors. *ACS Sens.* **2022**, *7* (1), 286−295.

https://doi.org/10.1021/acssensors.3c01638
ACS Sens. XXXX, XXX, XXX−XXX